BEST AVAILABLE IMAGES

Defective images within this document are accurate representations of the original documents submitted by the applicant.

Defects in the images may include (but are not limited to):

- BLACK BORDERS
- TEXT CUT OFF AT TOP, BOTTOM OR SIDES
- FADED TEXT
- ILLEGIBLE TEXT
- SKEWED/SLANTED IMAGES
- COLORED PHOTOS
- BLACK OR VERY BLACK AND WHITE DARK PHOTOS
- GRAY SCALE DOCUMENTS

IMAGES ARE BEST AVAILABLE COPY.

As rescanning documents *will not* correct images, please do not report the images to the Image Problem Mailbox.

ELSEVIER

Materials Science and Engineering A196 (1995) 253–260

MATERIALS SCIENCE & ENGINEERING A

Microstructures of laser-treated $Al_2O_3-ZrO_2-CeO_2$ composites

Zan-Hwey Chen, New-Jin Ho, Pouyan Shen

Institute of Materials Science and Engineering, National Sun Yat-Sen University, Kaohsiung, Taiwan

Received 14 February 1994; in revised form 12 September 1994

Abstract

This work uses room temperature X-ray diffraction and electron microscopy to investigate the effect of CO_2 laser treatments (800–2000 W, 10–15 s) on phase transformations and microstructural modification of sintered (1600 °C, 4 h) disks $A_xZ_yC_z$ (where A, Z and C denote Al_2O_3, ZrO_2 and CeO_2 respectively, and the subscripts represent molar ratios). Laser treatments under these conditions caused melting and more or less sublimation of all the samples; subsequent solidification and condension (predominant for CeO_2-rich composition) resulted in different microstructures between the samples. Dendritic and cellular domain structures due both to eutectic growth of α-Al_2O_3 and ZrO_2-CeO_2 solid solution were found in specimens $A_{30}Z_{63}C_7$ and $A_{70}Z_{27}C_3$ respectively. In the CeO_2-rich specimen $A_{40}Z_{12}C_{48}$ a drastic effect of condensation caused dendritic clusters of CeO_2 cubes (fluorite structure with minor amount of ZrO_2 and Al_2O_3 in solid solution) which overlaid on an Al_2O_3-rich matrix, predominantly $CeAlO_3$. Condensation through a rapidly solidifying liquid caused incorporation of Al_2O_3 in the fluorite structure and hence deviation from the octahedral shape predicted by the periodic bond chain model. Solute (Al_2O_3) trapping also suppressed the martensitic transformation of tetragonal (t-) to monoclinic (m-) ZrO_2 as manifested by the dendritic t-ZrO_2 cooled from the $Al_2O_3-ZrO_2$ eutectic. Laser treatment increased the Ce^{2+}/Ce^{4+} ratio and hence darkened the samples.

Keywords: Microstructure; Laser treatment; $Al_2O_3-ZrO_2-CeO_2$ composites

1. Introduction

The CO_2 laser provides a powerful heat source for surface and/or microstructural modifications of zirconia-bearing ceramics used for thermal barrier coatings (TBCs) [1–4]. Upon melting, the coating compositions determine the proportions of the liquid and vapor phases, and hence the subsequent solidification and/or condensation behavior. Little is known in this aspect for partially stabilized zirconia (PSZ) and zirconia dispersed ceramic (ZDC), which have been extensively studied near equilibrium conditions [5–7].

Under equilibrium, it has been quite well established that PSZ has considerable solid solubility, and hence tetragonal (t-) ZrO_2 precipitates coherently from the cubic (c-) ZrO_2 matrix [6], whereas for ZDCs such as $ZrO_2-Al_2O_3$, the solubility is rather limited and hence a composite with incoherent interface is obtained [7].

When deviation from equilibrium occurs, as in the case of laser remelting, several points need to be clarified for PSZs and ZDCs. These are: (1) a possible widening of the solid solubility, which affects phase trnsformations of the ZrO_2; (2) the effect of departure from eutectic composition on the microstructures of the rapidly solidified composites; (3) suitable compositions for a drastic condensation process which modify the surface of the composites; (4) color change due to transition metal oxide added as a stabilizer of ZrO_2. In this connection the results of recent studies are interesting, which indicated that addition of alumina during the laser surface melting process led to controlled microcracking and produced a surface alumina–zirconia eutectic, beneficial both to the strength[8] and the chemical resistance [9].

To meet the above interests, binary compositions of $Al_2O_3-ZrO_2$ and ZrO_2-CeO_2, and ternary compositions of $Al_2O_3-ZrO_2-CeO_2$ were selected for this study. The reasons for choosing this system are: (1) both PSZs and ZDCs are involved; (2) sufficient data about phase equilibria are available [10–12]; (3) there is rather a limited solid solubility in the $Al_2O_3-ZrO_2$ system [11], i.e. it is suitable for testing the possible

Elsevier Science S.A.
SSDI 0921-5093(94)09698-8

Table 1
Laser parameters and resultant phases of samples

	Laser treatments	Phases[a]
$A_{99}Z_1$	1.5 kW, 10 s	α-Al_2O_3, m-ZrO_2
$A_{62}Z_{38}$[b]	1.5 kW, 10 s	α-Al_2O_3, m-ZrO_2, t-ZrO_2
	2 kW, 15 s	α-Al_2O_3, m-ZrO_2, t-ZrO_2
A_1Z_9	1.5 kW, 10 s	α-Al_2O_3, m-ZrO_2
Z_9C_1	1.2 kW, 30 s	m-ZrO_2, t-ZrO_2
	2 kW, 10 s	m-ZrO_2, t-ZrO_2
Z_2C_8	2 kW, 10 s	CeO_2 s.s.[c] CeO_2
$Z_{76}C_{24}$[b]	1.5 kW, 15 s	CeO_2 s.s.
Z_6C_4	1.5 kW, 10 s	CeO_2 s.s.
$A_{70}Z_{27}C_3$	1.5 kW, 10 s	α-Al_2O_3, m-ZrO_2, t-ZrO_2
	2 kW, 10 s	α-Al_2O_3, m-ZrO_2, t-ZrO_2
$A_{30}Z_{63}C_7$	1.5 kW, 10 s	α-Al_2O_3, m-ZrO_2, t-ZrO_2
	2 kW, 10 s	α-Al_2O_3, m-ZrO_2, t-ZrO_2
$A_{40}Z_{12}C_{48}$	0.8 kW, 20 s	$CeAlO_3$, CeO_2 s.s.

[a] Identified by XRD (other phases may exist in trace amount).
[b] Eutectic compositions.
[c] CeO_2 s.s. denotes extensive solid solution with ZrO_2; other phases also form solid solution but to a lesser extent.

widening of solid solubility upon rapid solidification; (4) the ratio of Ce^{3+} to Ce^{4+} and hence the color change is sensitive to composition and temperature [13]; (5) a considerable amount of vapor is expected for CeO_2-rich compositions upon laser melting.

2. Experimental

Table 1 lists the compositions of samples $A_xZ_yC_z$, where A, Z and C denote Al_2O_3, ZrO_2 and CeO_2 respectively, and the subscripts represent molar ratios. Powders of Al_2O_3 (Elecmat 99.99% pure, < 1 μm in size), ZrO_2 (Cerac 99.9% pure, < 325 mesh) and CeO_2 (Cerac 99.9% pure, < 325 mesh) in selected ratios were ball-milled (Al_2O_3) to prepare mixture patches ≈ 0.8–1.1 g in weight and dry pressed at 100 MPa into disks ≈ 10 mm in diameter and 3 mm in thickness. All specimens were sintered at 1600 °C for 4 h and cooled in an open-air furnace. The cooling from 1600 °C to 1200 °C took about 10 min. The sintered disks were then subjected to CO_2-laser (PRC, FH-3000, 10.6 μm wavelength, beam mode TEM_{00+01^*}) treatments in a range of power input (800–2000 W) and time period (10–30 s) as shown in Table 1. A copper slab (a good reflector with respect to the laser beam) with a hemispherical hole ≈ 20 mm in diameter was used to hold the samples, which became more or less spheroid during laser treatments. Subsequent cooling of the samples to below incandescence took seconds. It was noted that preheating at a lower power input than the set value was required especially for CeO_2-rich specimens to avoid flipping of the sample disks.

The sintered or laser-treated specimens were pulverized and studied by X-ray diffractometer (Cu Kα, 35 kV, 25 mA, step scanning from 20° to 80° at 0.05° increment and 2 s per step) to identify the phases. Step scanning from 71° to 77° at 0.02° increment and 169 s per step was also adopted to identify the {400} of t-ZrO_2 and/or c-ZrO_2 phase in samples of eutectic Al_2O_3–ZrO_2 composition. The content of m- relative to c- and/or t-ZrO_2 was estimated from {111} peaks following the method of Ref. [14]. Scanning electron microscopy (SEM, JEOL6400 at 20 kV and JSM35CF at 25 kV) was used to study the sections or free surfaces of the laser-treated specimens. Backscattered electron imaging (BEI) coupled with energy dispersive X-ray (EDX) analysis were used to show the qualitative composition of the individual phases.

3. Results

3.1. Color and shape change

In the as-sintered condition, the CeO_2-free specimens were white in color, but those with CeO_2 appeared orange. Upon laser irradiation the latter generally melted at a lower power input (< 1000 W) than the former. After laser treatment, the former remained white and the shape became more or less spheroidal, whereas the latter changed to dark color and the shape became irregular. The color revived when the specimens were subjected to further heating (8 h at 1000 °C) in an open-air furnace.

The sintered samples were vaporized to a varied extent upon laser irradiation. Vaporization was dramatic for the CeO_2-rich samples: for example, in $A_{40}Z_{12}C_{48}$, the vapor that has been trapped in the early condensed and/or solidified matter erupted to form openings and fissures. The irregular shape of the CeO_2-rich samples and their faceted crystal clusters as shown later were caused predominantly by this vapor phase.

3.2. Solid solution and phase assemblages

X-ray diffraction (XRD) indicated that the phase assemblages of the sintered specimens are in accord with the 1600 °C isotherm of Ref. [12] (Fig. 1), but the equilibrium t-ZrO_2 in the ZrO_2–Al_2O_3 binary transformed into m-ZrO_2 upon cooling. In general, laser melting usually produced a solid solution among the oxides, according the EDX analyses. Considerable solid solution of foreign cations in zirconia caused a smaller d-spacing than that of pure ZrO_2. On the other hand, the incorporation of impurities was rather limited in Al_2O_3 as indicated by its having nearly the same d-spacings as α-Al_2O_3. In Table 1, the laser parameters and resultant phases of the various specimens are compiled. Laser treatments significantly modified the phase assemblages of some specimens, as shown below.

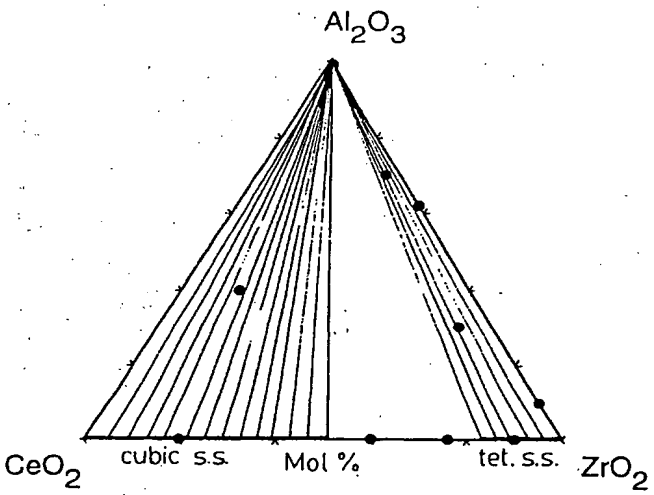

Fig. 1. Al_2O_3–ZrO_2–CeO_2 phase diagram at 1600 °C, after Ref. [12]. Solid circles represent compositions studied in this work.

The A_xZ_y specimens subjected to laser treatments contain α-Al_2O_3 (corundum structure) and ZrO_2, which appeared as m- and t-symmetry for eutectic composition $A_{62}Z_{38}$ (Fig. 2(a)), but as m-ZrO_2 for other compositions (Figs. 2(b) and 2(c)). It should be noted that the as-sintered $A_{62}Z_{38}$ specimen contained m-, not t-ZrO_2: thus laser melting of the eutectic had stabilized t-ZrO_2, ≈14% according to XRD (Table 2). Laser melting also caused a smaller d-spacing of m-ZrO_2.

Table 2
{111} d-spacings (in nm) of zirconia and percentage[a] of t-ZrO_2 for sample $A_{62}Z_{38}$

Conditions	$(11\bar{1})$ m-ZrO_2	(111) t-ZrO_2	% of t-ZrO_2
As sintered	0.3170	Not observed	Null
Laser treated, 1.5 kW, 10 s	0.3152	0.2954	14
Laser treated, 2 kW, 15 s	0.3156	0.2955	14

[a] Following the method of Ref. [14]

As for the Z_yC_z specimens treated by laser, ceria with zirconia in solid solution (designated as CeO_2 s.s. or Css) were identified by XRD (Fig. 3). The zirconia-rich specimen Z_9C_1 contains t- and m-ZrO_2 according to {111} (Fig. 3(a)) and {400} peaks (by step scanning, not shown). The CeO_2 s.s. has a cubic fluorite structure whose d-spacing increases with CeO_2 content (Figs. 3(b)–(d)). It should be noted that an additional cubic fluorite phase with a much larger cell volume (viz.

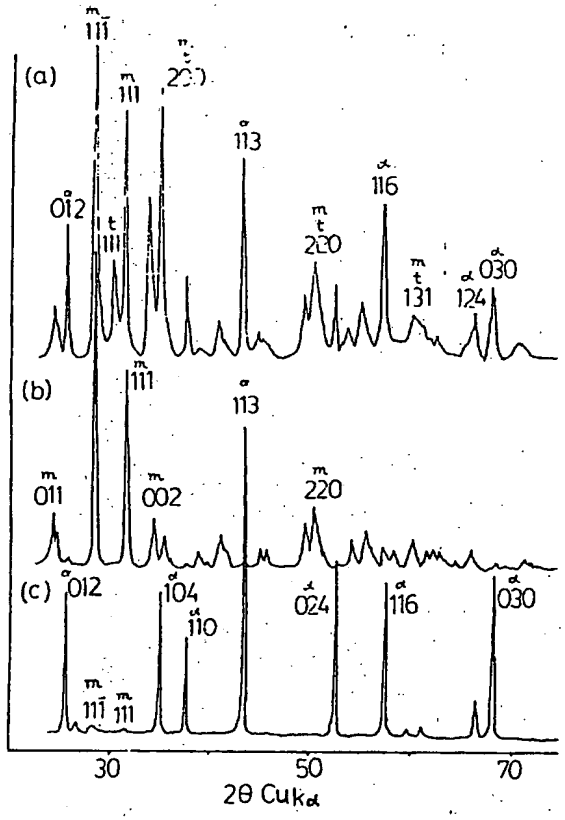

Fig. 2. XRD traces of A_xZ_y specimens treated by laser: (a) $A_{62}Z_{38}$, 2 kW for 10 s; (b) A_1Z_9, 1.5 kW for 10 s; (c) $A_{99}Z_1$, 1.5 kW for 10 s. Notation: α, t and m are α-Al_2O_3, t-ZrO_2 and m-ZrO_2, respectively.

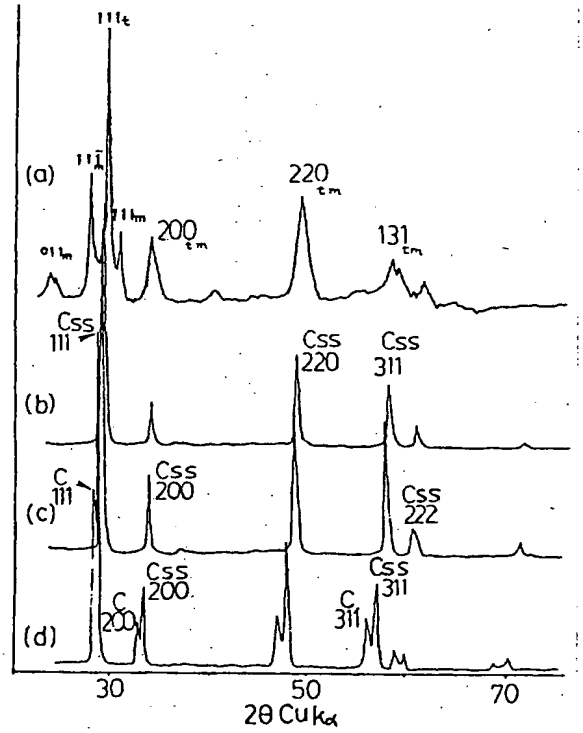

Fig. 3. XRD traces of A_xZ_y specimens treated by laser: (a) Z_9C_1, 2 kW for 10 s; (b) $Z_{76}C_{24}$, 1.5 kW for 10 s; (c) Z_6C_4, 1.5 kW for 10 s; (d) Z_2C_8, 2 kW for 10 s. Notation: Css and C are CeO_2 s.s. and CeO_2 respectively.

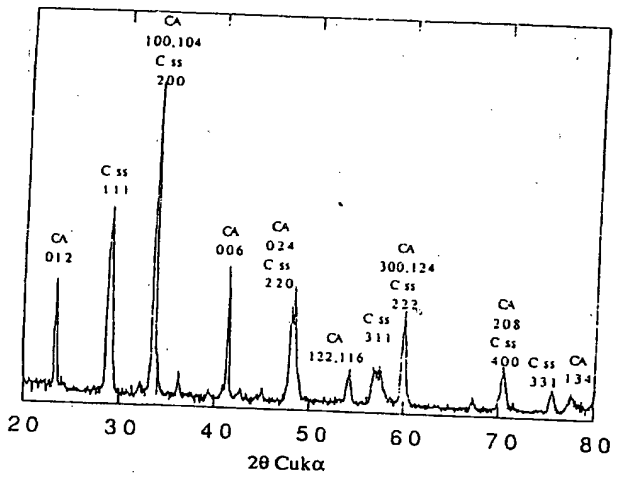

Fig. 4. XRD trace of $A_{40}Z_{12}C_{48}$ specimen treated by laser (0.8 kW for 20 s) CA and Css denote $CeAlO_3$ and CeO_2 s.s. respectively.

ceria-rich designated as C phase) appeared for the Z_2C_8 specimen when laser-treated at 2 kW for 10 s (Fig. 3(d)).

In $Al_2O_3-ZrO_2-CeO_2$ specimens treated by laser, the ZrO_2-CeO_2 solid solution always appeared; the α-Al_2O_3 remained in specimens $A_{70}Z_{27}C_3$ and $A_{70}Z_{27}C_3$ and $A_{30}Z_{63}C_7$ (not shown), but reacted with CeO_2 to form $CeAlO_3$ in specimen $A_{40}Z_{12}C_{48}$ (Fig. 4). As for the identity of the fluorite phase, the last specimen contains predominantly CeO_2 s.s., whereas the former two contain m-ZrO_2 and t-ZrO_2.

Change of the laser parameters (1000–2000 W, 10–20 s) did not cause an appreciable deviation of the phase assemblages, the d-spacings of ZrO_2 or the fraction of m-ZrO_2 in total ZrO_2, as shown by specimens $A_{62}Z_{38}$, $A_{70}Z_{27}C_3$, $A_{30}Z_{63}C_7$ or Z_9C_1 (Table 1).

3.3. Microstructures

Dendrites were recognized in the backscattered electron image (BEI) of all the specimens subject to laser treatment. In areas adjacent to the copper holder, the dendrites were finer with primary dendrites aligned preferentially along the temperature gradient. BEI coupled with EDX analysis indicated that the dendrites consisted of bright ZrO_2 and/or CeO_2 arms in the dark matrix of Al-rich phase (Al_2O_3 and/or $CeAlO_3$) which were more or less in solid solution with each other. Dendritic microstructures are depicted below for specimens $A_{30}Z_{63}C_7$, $A_{70}Z_{27}C_3$ and $A_{40}Z_{12}C_{48}$ which represent off-eutectic, near-eutectic and CeO_2-rich compositions respectively, all in the two-phase region of the 1600 °C isotherm [12]. In general, the dendrites and eutectic domains of these specimens were better developed at a higher power input.

3.3.1. Off-eutectic

Near the edge of the specimen $A_{30}Z_{63}C_7$, ZrO_2 s.s. formed nonfaceted dendrites in the Al_2O_3-rich matrix, and the primary arms of dendrites extended hundreds of micrometres inwards (Fig. 5(a)). In the interior of the specimen, broken but coarser ZrO_2 arms were formed in the Al_2O_3 matrix (Fig. 5(b)); occasionally a two-phase eutectic texture consisting also of nonfaceted ZrO_2 in a matrix of Al_2O_3 was recognized (Fig. 5(c)).

3.3.2. Eutectic

The eutectic texture of ZrO_2 s.s. in Al_2O_3 matrix appeared to be slightly dendritic near the edge of the specimen $A_{70}Z_{27}C_3$ after laser melting at 2 kW for 10 s (Fig. 6(a)). Cellular domains up to 200 μm in domain size were well developed in the interior of this specimen (Fig. 6(b)). In the individual domains, Al_2O_3 cells or

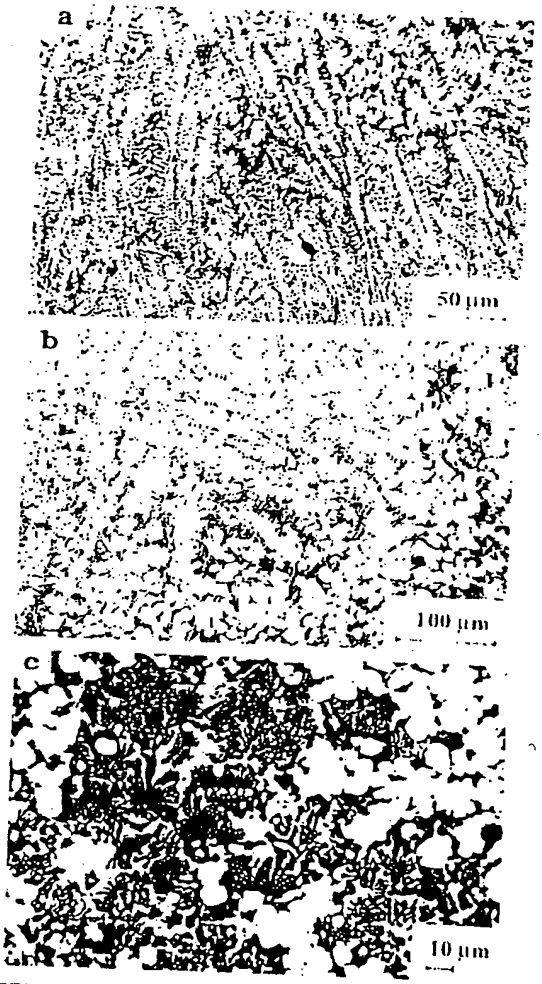

Fig. 5. SEM images (BEI) of specimen $A_{30}Z_{63}C_7$ treated by laser (2 kW for 10 s) showing: (a) nonfaceted ZrO_2 s.s. dendrites (bright) in the Al_2O_3-rich matrix (dark), which extend inward from the edge of the specimen; (b) separated but coarser ZrO_2 crystals; (c) eutectic texture in the interior of the specimen.

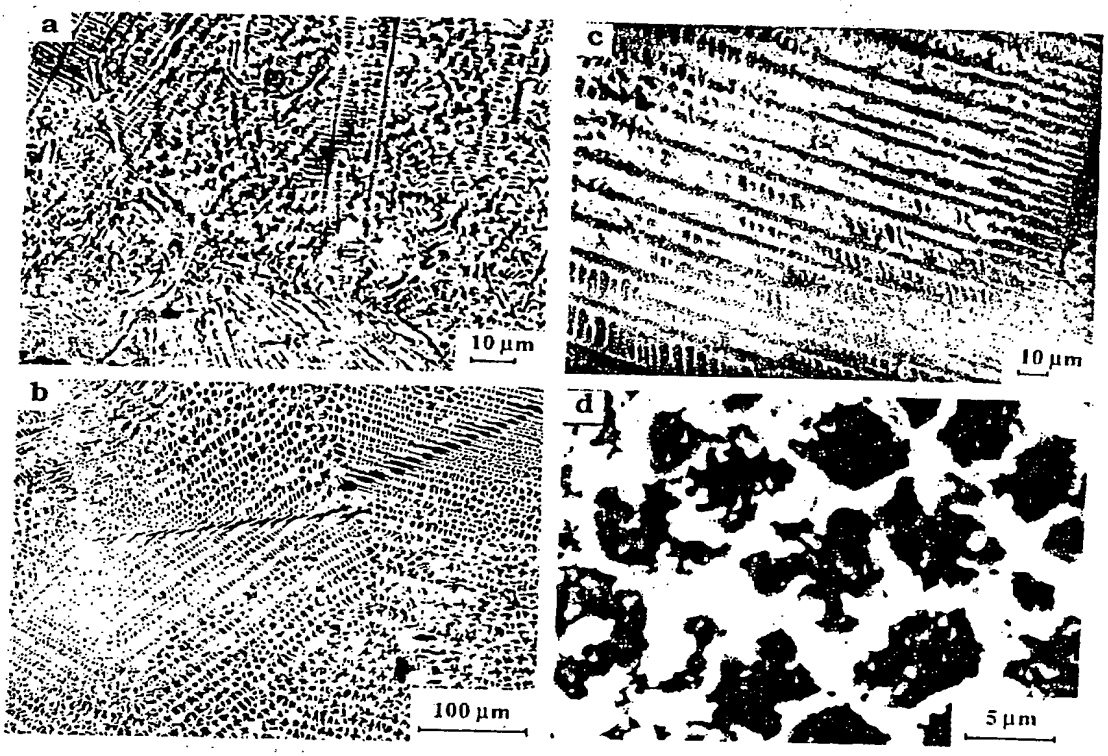

Fig. 6. SEM images (BEI) of specimen $A_{70}Z_{27}C_3$ treated by laser (2 kW for 10 s) showing eutectics consisting of ZrO_2 s.s. (bright) and Al_2O_3 (dark): (a) near the edge in contact with copper; (b) domains of cellular structure in the interior of the specimen; (c) the Al_2O_3 s.s. form separated cells or rods surrounded by ZrO_2 s.s. rims or vice versa in the individual domain; (d) head-on view of eutectic domain cells formed at 1.5 kW and 10 s.

rods were surrounded by ZrO_2 s.s. rims or vice versa (Fig. 6(c)). The cells of the eutectic domain were similar when formed under a lower power input (1.5 kW and 10 s). It is noteworthy that the interphase interface is nonfaceted in both the side view (Figs. 6(a)–6(c)) and the head-on view (Fig. 6(d)).

3.3.3. CeO_2-rich composition

BEI of the interior of the specimen $A_{40}Z_{12}C_{48}$ (Fig. 7(a)) revealed broken arms of nonfaceted CeO_2–ZrO_2 s.s. (bright) and faceted $CeAlO_3$ (grey). Near the fissure or opening of the specimens where vapor was emitted, skeletal dendrites consisting of CeO_2 cubes were recognized (Fig. 7(b)). Secondary electron imaging (SEI) revealed the surface of the cubes in detail (Fig. 8). The cubes when magnified and tilted to near ⟨111⟩ orientation appeared to be smooth on {100} at the scale of micrometres, except for the local area marked with an arrow (Fig. 8). SEI of the same composition but treated at a higher power input (2 kW) revealed CeO_2 cubes in colonies, and the individual cubes preferentially grew at their corners and edges (Fig. 9). Each crystal colony resembles the classical dendrite, but more isometric and skeletal. Note that these CeO_2 cubes preferentially aligned along ⟨200⟩ regardless of the power input adopted. EDX analysis indicated that the CeO_2 cubes contain less Al than $CeAlO_3$.

4. Discussion

4.1. Color change due to CeO_2

A solid solution of ZrO_2–CeO_2 [15,16] or UO_2–CeO_2 [17] changed to a dark color by various processes at high temperatures where a considerable amount of Ce^{3+} is stable. In the solid solution of ZrO_2–CeO_x (where x denotes deviation from 2), the Ce^{3+} content is the largest ($\approx 66\%$ $Ce^{3+}/(Ce^{3+} + Ce^{4+})$) for a composition with ≈ 30 mol.% CeO_x [13]. The Ce^{3+} could be co-introduced with oxygen vacancies by the following equation [18]:

$$2Ce_{Ce^x} + O_{O^x} \rightarrow 2Ce_{Ce'} + V_{OO}^{\cdot\cdot} + \frac{1}{2O_2}(g) \quad (1)$$

where the Kroger–Vink notation is adopted [19]. The partially filled filled f shells of Ce^{3+} account for the color change in various minerals [20] and may be extended to the present CeO_2-bearing specimens. This suggestion is supported by the fact that the color change is more marked for specimens $Z_{74}C_{24}$ and Z_6C_4 than Z_2C_8, whose Ce^{3+} content, i.e. $Ce^{3+}/(Ce^{3+} + Ce^{4+})$, are about 65, 62 and 38% respectively at high temperatures [13]. Further evidence of the role of Ce^{3+} in the color change is the color revival upon

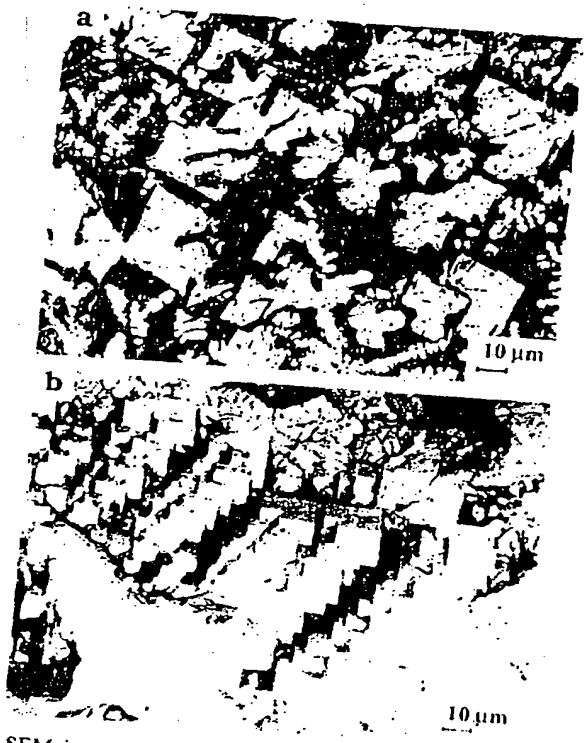

Fig. 7. SEM images (BEI) of specimen $A_{40}Z_{12}C_{48}$ treated by laser (0.8 kW for 10 s) showing (a) nonfaceted and isolated CeO_2–ZrO_2 s.s. (bright) dendrites and faceted $CeAlO_3$ (grey) formed by solidification in the interior of the specimen; (b) dendritic CeO_2 s.s. cubes in the matrix of $CeAlO_3$ formed by both condensaton and solidification near the fissures or openings of the specimen.

heating these specimens in an open-air furnace at 1000 °C for 8 h (i.e. the opposite of Eq. (1)). Other transition metal oxides that are commonly reduced by CeO_2 to modify colors of glass ceramics [21] were negligible in the present powder batches. It should be noted that $CeAlO_3$ in the laser-treated specimen $A_{40}Z_{12}C_{48}$ remained dark when subject to further heating at 1000 °C for 8 h in an open-air furnace, indicating that reaction (1) was negligible for such a compound.

Fig. 8. SEM image (SEI) of CeO_2 s.s. cubes magnified and tilted from Fig. 7(b) to show impingement of cubes at corners and three {100} faces, which appeared to be flat with some ledges (arrow).

Fig. 9. SEM image (SEI) of skeletal CeO_2 s.s. grown at corners and/or edges of the individual cubes: free surface of specimen $A_{40}Z_{12}C_{48}$ treated by laser (2 kW for 10 s).

4.2. Formation of CeO_2 cubes

Supersaturation of vapors in terms of T_1/T_m is the important driving force for the condensation of metals [22], where T_1 represents the temperature for vapor to reach 1 Torr and T_m is the melting point. In general, a low value of T_1/T_m (e.g. 0.9–1.54 for most metals studied [22]) is required for a condensation process. This consideration appeared to be applicable to CeO_2 cubes in view of the serious evaporation of the CeO_x-rich composition [13] and the fact that CeO_2 with a slight amount of Al_2O_3 in solid solution indeed formed at the free surface of the specimen $A_{40}Z_{12}C_{48}$. The skeletal crystals have been suggested to be characteristic of crystal growth from the liquid phase at high deviations from equilibrium [23]. A VLS (abbreviations denote vapor, liquid and solid respectively) mechanism [24,25], but with a small wetting angle or a large amount of liquid to avoid whisker growth, may account for the condensation of skeletal CeO_2.

It is of interest to note that CeO_2 cubes with {100} faces were formed, in contrast to the {111} octahedron observed previously for CeO_2 grown from a flux [26] or predicted by the periodic bond chain (PBC) model [27,28]. According to this model, {111} of the fluorite structure belongs to F faces which have more than two PBCs, and therefore has the lowest surface energy, whereas {100} belongs to K faces which have no PBC. Deviation of crystal forms from PBC prediction can be explained by impurities, which modify the attachment energy of individual atoms [28]. The presence of impurities may also enhance material supply to the corners and edges of growing crystals, and preferential nucleation in these areas (due to the ionic character of the crystals) is considered to be principal factor in skeletal growth [29]. It remains to be clarified whether Al^{3+}, which dissolves slightly in CeO_2 does indeed affect the

growth behavior. Further study of the shape of CeO_2 crystals condensed directly from laser-induced vapors may shed light on this point.

4.3. Al_2O_3-stabilized t-ZrO_2

The solubility of Al_2O_3 in ZrO_2 is small: e.g. less than 1 mol.% at 1600 °C [11]. Therefore, unless it is co-doped with other cations [30], oxygen vacancies introduced to maintain electron neutrality are not enough to stabilize c- and/or t-ZrO_2 at room temperature, as shown by the sintered $Al_{62}Z_{38}$ specimen. Laser melting and rapid solidification, however, expanded the solid solubility metastably, resulting in smaller d-spacings of m-ZrO_2 and the stabilization of t-ZrO_2 (Table 2). Substitution of Zr^{4+} with a coordination number (CN) of 8 by Al^{3+} is expected to cause a smaller cell volume of ZrO_2, although no ionic radii of Al^{3+} ion are available with such a CN [31]. It should be noted that a solid solution of Al_2O_3 in the ZrO_2–CeO_2 s.s. also caused a smaller cell volume, in accordance with a smaller cation of Al^{3+} than the cations of Zr or Ce (Table 3).

In addition to being a stabilizer, Al_2O_3 may also exert volume constraint on ZrO_2 to reduce the martensitic transformation temperature (M_s), i.e. stabilizing t-ZrO_2 as for the ZDCs [5,7]. The possibility, however, is excluded for the present case because t-ZrO_2 survived pulverizing of the laser-treated $Al_{62}Z_{38}$ specimen.

Since Al^{3+}-bearing t-ZrO_2 was found in the binary Al_2O_3–ZrO_2 with eutectic composition (i.e. $Al_{62}Z_{38}$, but not $A_{99}Z_1$ or A_1Z_9) and subject to laser melting, rapid solidification of an eutectic melt is essential for the incorporation of Al^{3+} in ZrO_2. A solute-trapping process, which was suggested to be valid at the solid/liquid interface of a rapidly solidifying alloy [32], may account for the widening of the solid solubility of the ceramic materials. It should be noted, however, that cations of Zr and/or Ce did diffuse significantly into the z-Al_2O_3 lattice in such a process. Further study by analytical electron microscopy is required to identify a possible composition spike or local equilibrium, which are relevant to a solute-trapping process.

Table 3
Ionic radii[a] of elements in coordination numbers of 8 and 6

Elements	Ionic radius (nm)	Misfit with respect to Zr^{4+}
Zr^{4+} (8)[b]	0.084	Null
Ce^{3+} (8)	0.1143	+36%
Ce^{4+} (8)	0.097	+15%
Zr^{4+} (6)	0.072	Null
Ce^{3+} (6)	0.101	+40%
Ce^{4+} (6)	0.087	+21%
Al^{3+} (6)	0.0535	−26%

[a] After Shannon [31].
[b] Numbers in parentheses are coordination numbers.

4.4. Implications

Taking advantage of the high density of power input of CO_2 laser and the high rate of heat transfer by a metal holder, rapid solidification and/or condensation of the refractory ceramics can be accomplished as demonstrated in the present composition system. A variety of colors, microstructures (dendrites, eutectic domains and faceted crystals) and phase assemblages can then be produced by the combined effects of temperature, composition, vapor pressure, surface energy and other kinetic factors. The solid solubility of a phase can also be expanded metastably by laser melting, as demonstrated by the incorporation of Al^{3+} in ZrO_2, and hence the suppression of the t → m transformation. Laser treatments appeared to be useful also for the habit modification of ceramic crystals, such as the unusual cubes of CeO_2 formed by condensation through a liquid phase. Properties of a laser-sealed coating may rely greatly on its microstructure for example, a controlled microcracking and a surface alumina–zirconia eutectic has been found to be beneficial to both the strength [8] and the chemical resistance [9]. The dendritic and/or eutectic domains of Al_2O_3/ZrO_2 composites as revealed in the present study may arrest microcracking and suppress oxidation (ZrO_2 is basically transparent to oxygen at high temperatures) because of the high specific area of the interphase interface.

5. Conclusions

X-ray diffraction and electron microscopy studies of laser-melted Al_2O_3–ZrO_2–CeO_2 composites (designated as $A_xZ_yC_z$, where A, Z and C denote Al_2O_3, ZrO_2 and CeO_2 respectively, and the subscripts represent molar ratios) led to the following conclusions.

(1) Laser melting and subsequent solidification caused extensive formation of dendrites in all the specimens.

(2) Dendritic and cellular domain structures, both due to syntaxial growth of Al_2O_3 and ZrO_2–CeO_2 solid solution, were found in specimens $A_{30}Z_{63}C_7$ and $A_{70}Z_{27}C_3$ respectively.

(3) Dendritic clusters of CeO_2 cubes (c-fluorite structure with minor amount of Al_2O_3 in solid solution) appeared in the Ce-rich specimen $A_{40}Z_{12}C_{48}$. The combined factors of solidification, condensation and interface kinetics, such as the interaction of defects and bonding at the surface, probably account for the formation of skeletal cubes rather than octahedrons.

(4) Rapid solidification caused Al_2O_3 trapping in the ZrO_2 lattice and hence stabilization of the t-ZrO_2 phase.

(5) Laser treatment increased the Ce^{3+} to Ce^{4+} ratio and hence darkened the specimens.

References

[1] K.M. Jasim, R.D. Rawlings and D.R.F. West, *J. Mater. Sci., 25* (1990) 4943.
[2] M. Okutomi, *Mater. Manuf. Proc., 6* (1991) 139.
[3] J.H. Shieh and S.T. Wu, *Appl. Phys. Lett., 59* (1991) 1512.
[4] W.B. Lin, P. Shen and N.J. Ho, in *Proc. Annual Conf. Chinese Soc. Mater. Sci., Taipei, 1992*, p. 574.
[5] M. Ruhle and A.H. Heuer, in N. Claussen, M. Ruhle and A.H. Heuer (eds.), *Science and Technology of Zirconia II, Advances in Ceramics*, Vol. 12, The American Ceramic Society, Columbus, OH, 1984, p. 14.
[6] A.H. Heuer and M. Ruhle, in N. Claussen, M. Ruhle and A.H. Heuer (eds.), *Science and Technology of Zirconia II, Advances in Ceramics*, Vol. 12, The American Ceramics Society, Columbus, OH, 1984, p. 1.
[7] A.H. Heuer, N. Claussen, W.M. Kriven and M. Ruhle, *J. Am. Ceram. Soc., 65* (1982) 642.
[8] A. Petitbon, D. Guignot, U. Fischer and J.M. Guillemot, *Mater. Sci. Eng., A121* (1989) 545.
[9] A. Petitbon, L. Boquet and D. Delsart, *Surf. Coat. Technol., 49* (1991) 57.
[10] P. Duran, M. Gonzalez, C. Moure, J.R. Jurado and C. Pascual, *J. Mater. Sci., 25* (1990) 5001.
[11] A.M. Alper, in G.H. Stewert (ed.), *Science of Ceramics*, Vol. 3, Academic Press, 1976, p. 339.
[12] V. Longo and L. Podda, *Ceramurgia, 1* (1971) 11.
[13] A. Rouanet, *C.R. Acad. Sci. Paris Ser. C., 226* (1968) 908.
[14] H. Toraya, M. Yoshimura and S. Somiya, *J. Am. Ceram. Soc., 67* (1984) C-119.
[15] J.R. Brandon and R. Taylor, *Surf. Coat. Technol., 46* (1991) 91.
[16] G.A. Rossi, in S. Meriani and C. Palmonari (eds.), *Advances in Zirconia Science and Technology*, Elsevier Applied Science, 1989, p. 271.
[17] M.C. Pienkowski, M.L. Jenkins and P.T. Moseley, *J. Solid State Chem., 92* (1991) 543.
[18] I. Reiss, H. Janczikowski and J.N. Ting, *J. Appl. Phys., 61* (1987) 4931.
[19] K. Nassau, *Am. Mineral., 63* (1978) 219.
[20] F.A. Kroger and H.J. Vink, *Solid State Phys., 3* (1956) 307.
[21] W. Vogel, *Chemistry of Glass*, The American Ceramics Society, Colombus, OH, 1985, p. 264.
[22] R. Uyeda, in I. Suunagawa (ed.), *Morphology of Crystals*, Part (B), Terra Sci. and D. Reidel Co., Tokyo, 1987, pp. 367–508.
[23] G.G. Lemmlein, M.O. Kliya and A.A. Chernov, *Sov. Phys. Crystallogr., 9* (1964) 181.
[24] R.S. Wagner and W.C. Ellis, *Appl. Phys. Lett., 4* (1964) 89–90.
[25] E.I. Givargizov, in *Highly Anisotropic Crystals* (English edition by M. Senechal), Terra Sci. and D. Reidel Co., Tokyo, 1987, pp. 20–229.
[26] R.C. Linares, *J. Phys. Chem. Solids, 28* (1967) 1285.
[27] P. Hartman and W.G. Perok, *Acta Crystallogr., 8* (1955) 49, 521, 525.
[28] P. Hartman, in I. Sunagawa (ed.), *Morphology of Crystals*, Part A, Terra Sci. and D. Reidel Co. Tokyo, 1987, p. 271, and references cited therein.
[29] E.I. Givargizov, in *Highly Anistropic Crystals* (English edition by M. Senechal), Terra Sci. and D. Reidel Co., Tokyo, 1987, pp. 230–251.
[30] S. Chen, W. Deng and P. Shen, *Mater. Sci. Eng. B, 22* (1994) 247.
[31] R.D. Shannon, *Acta Crystallogr., Sect. A, 32* (1976) 751.
[32] J.C. Baker and J.W. Cahn, *Acta Metall., 17* (1969) 575.